Plant Pathology

WILEY

Plant Pathology

ORIGINAL ARTICLE OPEN ACCESS

Revisiting the Evolution and Function of NIP2 Paralogues in the *Rhynchosporium* Spp. Complex

Reynaldi Darma[1,2] | Daniel S. Yu[1] | Megan A. Outram[1] | Ben Ovenden[3] | Yi-Chang Sung[1] | Erin H. Hill[1] | Daniel Croll[4] | Simon J. Williams[1] | Xuechen Zhang[3] | Andrew Milgate[3] | Peter S. Solomon[1] | Megan C. McDonald[1,5]

[1]Research School of Biology, The Australian National University, Canberra, Australian Capital Territory, Australia | [2]Department of Protecting Crops and the Environment, Rothamsted Research, Harpenden, UK | [3]NSW Department of Primary Industries, Wagga Wagga Agricultural Institute, Wagga Wagga, New South Wales, Australia | [4]Laboratory of Evolutionary Genetics, Institute of Biology, University of Neuchâtel, Neuchâtel, Switzerland | [5]School of Biosciences, Institute of Microbiology and Infection, University of Birmingham, Birmingham, UK

Correspondence: Megan C. McDonald (m.c.mcdonald@bham.ac.uk) | Peter S. Solomon (peter.solomon@anu.edu.au)

Received: 24 February 2025 | **Accepted:** 20 March 2025

Funding: This work was supported by the Grains Research and Development Corporation under the National barley foliar pathogen variety improvement programme (DAQ00187). R.D. was supported by The Australian National University scholarships and The British Society for Plant Pathology (BSPP) COVID-19 support.

Keywords: effectors | necrosis-inducing protein | NIP2 | paralogues | *Rhynchosporium commune*

ABSTRACT

The fungus *Rhynchosporium commune*, the causal agent of barley scald disease, contains a paralogous effector gene family called *Necrosis-Inducing Protein 2* (*NIP2*) and *NIP2-like protein* (*NLP*). However, the function and full genomic context of these paralogues remain uncharacterised. Here we present a highly contiguous long-read assembly of a newly isolated Australian strain, *R. commune* WAI453, that is virulent on multiple barley cultivars. Using this assembly, we show that the duplication of the *NIP2* and *NLP* gene families is distributed throughout the genome and pre-dates the speciation of *R. commune* from other species in the *Rhynchosporium* genus. Some *NIP2* paralogues have subsequently been lost or are absent in these closely related species. The diversity of these paralogues was examined from *R. commune* global populations and their expression was analysed during in planta and in vitro growth to evaluate the importance of these genes during infection. The majority of *NIP2* and *NLP* paralogues in the WAI453 genome were significantly upregulated during plant infection suggesting that the *NIP2* and *NLP* genes harbour virulence roles. An attempt to further characterise the function of NIP2.1 by infiltrating purified protein into barley leaves did not induce necrosis, questioning its previously reported role as an inducer of host cell death. Together these results suggest that the *NIP2* effector family does play a role during infection of barley; however, the exact function of *NIP2*, like many effectors, remains uncharacterised.

1 | Introduction

Rhynchosporium commune is the causal agent of barley scald disease, which can cause grain yield losses as high as 45% under favourable field conditions (Brown 1985; Zaffarano et al. 2011). In the United Kingdom, scald disease causes £7.2 million in yield and grain quality losses to the barley industry despite the use of intensive fungicide treatment programmes (Paveley et al. 2016). The predominant symptom of scald is large necrotic lesions on affected leaves with dark brown margins that reduce the photosynthetic leaf area and lead to significant yield losses (Avrova and Knogge 2012). *R. commune* can also infect barley ears, sometimes causing serious grain infections that reduce grain value (Avrova and Knogge 2012; Skoropad 1959; Zhan et al. 2008). Early studies of the *Rhynchosporium* genus described two different

species: *R. secalis*, which infected barley, rye and some species of wild grasses; and *R. orthosporum,* which infected orchard grass (Goodwin 2002). However, more recent analyses divided *R. secalis* into three different species: *R. commune*, which infects barley and other *Hordeum* spp.; *R. secalis*, which infects rye and triticale; and *R. agropyri*, which infects *Agropyron* spp. (Zaffarano et al. 2011). Later, a novel *Rhynchosporium* species was isolated from perennial ryegrass and was named *R. lolii* (King et al. 2013). *R. commune*, *R. secalis* and *R. agropyri* are classified as the beaked conidia group (BCG) are phylogenetically closely related and referred to as sister species (King et al. 2013; Penselin et al. 2016; Zaffarano et al. 2011). The remaining two species, *R. lolii* and *R. orthosporum*, are classified as the cylindrical conidia group (CCG) and form a separate phylogenetic group (King et al. 2013). Among these five species, *R. commune* and *R. secalis* are considered the most damaging with a global distribution, whereas the other species remain minor causing diseases primarily on pasture grass species (King et al. 2013; Paveley et al. 2016; Zaffarano et al. 2011).

Rhynchosporium commune is considered a hemibiotropic pathogen that has a long asymptomatic period (7–10 days) followed by the rapid appearance of large necrotic lesions (Avrova and Knogge 2012; Kirsten et al. 2012). This two-stage infection cycle is hypothesised to be driven by different sets of secreted effectors. In the first stages of infection, effectors that suppress plant immunity are hypothesised to be the main drivers of infection, which are then followed by a second set of necrosis-inducing effectors that damage plant tissues (Lu et al. 2022; Shao et al. 2021). To date, three effectors secreted by *R. commune* have been described following purification from in vitro culture filtrates. These proteins were named Necrosis-Inducing Proteins (NIP1, NIP2 and NIP3), as they were shown to induce necrosis when infiltrated into barley leaves (Wevelsiep et al. 1991). NIP1 and NIP3 were both shown to stimulate the host plant plasma membrane H^+-ATPase, whereas NIP2 was not found to affect ATPase activity (Wevelsiep et al. 1993). Despite the strong activity observed in these studies, no further work has been conducted to explore the mechanistic basis leading to plant necrosis.

The *NIP* effector gene family has since been expanded based on whole-genome resequencing studies of *R. commune*. Mohd-Assaad et al. (2019) recently reported the presence of two highly identical *NIP1* paralogues, now named *NIP1A* and *NIP1B*. Interestingly, these genes appear to not only exist as paralogues but also have copy number variation in different fungal isolates (Mohd-Assaad et al. 2019). In a global study, *NIP1A* was found more frequently in isolates when compared to *NIP1B*, and isolates containing a functional *NIP1A* were also found to be more virulent than those without this gene. *NIP1B* had a smaller but significant effect on virulence in isolates that carried two copies of this paralogue, suggesting that both effector presence/absence polymorphism and copy number variation can play a role in the virulence of this important pathogen (Mohd-Assaad et al. 2019).

Remarkably, *R. commune* carries 11 described *NIP2* paralogues (*NIP2.1–NIP2.11*), defined by three conserved motifs: a 40-amino acid sequence at the *N*-terminus, a 15-amino acid sequence containing three conserved amino acids (cysteine, arginine and serine [CRS]) in the middle of the protein sequence, and a C-terminal 15-amino acid sequence (Penselin et al. 2016). In addition to these three conserved motifs, these 11 paralogues also have six conserved cysteine residues. The *NIP2.1* gene also contains a unique intron in the 3 untranslated region (UTR) immediately following a stop codon (Kirsten et al. 2012). The presence of this 3 UTR intron in the other *NIP2* paralogues remains uncharacterised. Two more distantly related NIP2-Like Proteins (*NLPs*), NLP2 and NLP3, have also been described (Penselin et al. 2016). NLPs also share the six conserved cysteine residues found in NIP2 paralogues but are less conserved in the other NIP2 protein domains, most notably lacking the conserved CRS domain (Penselin et al. 2016).

Apart from NIP2.1 that was reported to induce necrosis on barley leaves (Wevelsiep et al. 1991), only one other paralogue, known as NIP2.6 (*RcSP6*), has been functionally investigated (Penselin et al. 2016). The virulence of an *RcSP6* knockout mutant was similar to that of the wild type, suggesting this gene does not have a role in inducing necrosis on barley leaves. However, the biomass of the mutant was more abundant than the biomass of the wild type, indicating this gene plays a role in suppressing fungal growth during the asymptomatic period of infection (Penselin et al. 2016). Together, these studies indicate that NIP2.6 and NIP2.1 have different functions within the *R. commune*–barley interaction. In this paper, we assessed the genomic context and evolutionary history of this expansive effector family in *R. commune*. We did this by generating a high-quality contiguous genome assembly and analysing the diversity of NIP2 paralogues from *R. commune* global populations and related species within the genus. We also examined the expression of the *NIP2* paralogue family in planta, to explore if the *NIP2* paralogues have diversified the timing of their expression during infection. Finally, we used heterologous expression to explore the reported necrosis-inducing activity of NIP2.1.

2 | Materials and Methods

2.1 | *R. commune* Strains, Fungal Genome Sequencing and Assembly

Seventy-two new Australian *R. commune* strains, labelled as the 'Australia_New' population, were collected by the New South Wales (NSW) Department of Primary Industries, Australia, in 2013–2018 as part of the Wagga Wagga Agricultural Institute Isolate Collection (Table 1). The Wagga Wagga Agricultural Institute Fungal Isolate Collection is an internationally significant repository of cereal pathogen and other fungal isolates collected from around Australia, housed at the NSW Department of Primary Industries and Regional Development facilities at Wagga Wagga Agricultural Institute. Five isolates, WAI453, WAI2439, WAI2471, WAI2473 and WAI2840, have been reported by Zhang et al. (2019). The remaining isolates are reported for the first time in this study. An additional 118 *R. commune* and closely related species genomes were sequenced by Mohd-Assaad et al. (2019) and listed by population in Table 1. This includes one historic Australian *R. commune* population, which is simply labelled as

TABLE 1 | List of 190 *Rhynchosporium commune* isolates used in this study.

Country	Code	Number of isolates	Reference
Australia	AU	12	McDonald et al. (1999)
Australia_New	AU_N	72	First described in this study, Zhang et al. (2019)
Switzerland	CH	11	Linde et al. (2003)
Ethiopia	ET	14	Linde et al. (2003)
Finland	FI	14	Salamati et al. (2000)
Iceland	IS	12	Stefansson et al. (2013)
Norway	NO	14	Salamati et al. (2000)
New Zealand	NZ	14	Linde et al. (2009)
Spain	SP	14	Stefansson et al. (2013)
USA	US	13	McDermott et al. (1989)

the 'Australian' population (McDonald et al. 1999). For long-term storage, spores of WAI453 were resuspended in 25% glycerol and stored at −80°C. The WAI453 strain was grown on 2% lima bean agar (filtrate of 125 g/L boiled lima bean, 20 g/L agar) and incubated at 18°C in darkness for 10 days. Spores were collected from agar plates and high-molecular weight (HMW) genomic DNA was extracted according to the methods described on protocols.io (Darma and McDonald 2019). The genomic DNA library prepared from the extracted HMW DNA was generated using a PacBio SMRTBell Template Prep Kit 1.0 SPv3 with BluePippin 15–50 kb size selection. The library was sequenced on a PacBio Sequel machine with sequel sequencing kit v. 2.1 chemistry at the Ramaciotti Centre (UNSW Sydney, NSW, Australia).

Raw PacBio sequencing reads were corrected, trimmed and de novo assembled with Canu v. 1.5 with the following settings: genomeSize = 57 m, minReadLength = 11,000, correctedErrorRate = 0.040 and stopOnReadQuality = false (Koren et al. 2017). This raw assembly was further polished with raw PacBio reads to obtain a more accurate assembly. To do this, the reads were first aligned to the raw assembly using BLASR v. 5.1 with the following settings: –hitPolicy randombest –minMatch 12 –nCandidates 2 –useQuality true –minReadlength 1000 –minSubreadLength 500 (https://github.com/BioinformaticsArchive/blasr). The raw assembly was subsequently polished with raw genomic reads using Variantcaller Arrow v. 2.3.2 with the following settings: –minConfidence 40 –minCoverage 25 –coverage 100 –minReadScore 0.75 (https://biocontainer-doc.readthedocs.io/en/latest/source/genomicconsensus/genomiconsensus.html).

Short-read sequencing was performed for the other 71 *R. commune* Australia_New isolates at The Australian Genome Research Facility (Westmead, NSW, Australia). The genomic DNA libraries were prepared using the Nextera DNA Flex kit and sequenced using the NovaSeq 6000 Illumina machine. The sequencing reads (100 bp, paired-end) were assembled using SPAdes v. 3.13 (Bankevich et al. 2012).

2.2 | Plant Infection and RNA Sequencing From In Planta and In Vitro Growth

Pathotyping for *R. commune* WAI453 was conducted using glasshouse seedling screens in 2018 and 2019. Seedlings were inoculated 10–14 days after sowing, at the three-leaf stage, with 200,000 spores/mL of WAI453. Seedlings were incubated at 100% relative humidity (RH) for 48 h at 18°C in the dark and then grown in a glasshouse in full sunlight at 21°C during the day and 13°C at night. Disease severity was assessed using the 1–5 seedling scale of Zhang et al. (2019) at 10–14 days post-inoculation (dpi). Three replicates of each barley variety were scored in 2018 and two replicates in 2019. These scores were used to formulate a seedling disease resistance rating for each cultivar.

For RNA sequencing, plant infection assays were performed on 3-week-old barley cv. ND5883 (Fetch and Steffenson 1994) grown in controlled environment growth chambers under a 14 h day/10 h night cycle (20°C day/12°C night) at 85% RH according to McDonald et al. (2018). A concentration of 10^6 spores/mL in 0.02% Tween 20 was sprayed on the top of the third leaves of 3-week-old barley seedlings. Infected seedlings were incubated in darkness at 18°C with 100% RH for 48 h before they were transferred to a growth chamber for an additional 6 days' incubation under normal plant growth conditions.

For in vitro growth, 50 mL of lima bean broth was inoculated with 10^6 spores of WAI453 and incubated in the dark with shaking (120 rpm) at 18°C for 8 days. Fungal mycelia and culture filtrate were separated with Miracloth (Merck). Infected leaves and fungal mycelia were snap frozen in liquid nitrogen and stored at −80°C before RNA extraction. RNA from three biological replicates of infected leaves and fungal mycelium was extracted using Quick-RNA Fungal/Bacteria Miniprep (Zymo Research) following the manufacturer's protocol. Eluted RNA was treated for genomic DNA contamination using TURBO DNase (Thermo Fisher). High-quality RNA from in vitro samples and in planta samples was used to construct Illumina stranded mRNA libraries. RNA samples with RNA integrity number (RIN) higher than 8.4 for in vitro samples and 5 for in planta samples were used for the construction of mRNA libraries. The RNA samples from in planta samples had lower RIN values than those of in vitro samples due to the presence of both nuclear and chloroplast rRNA in these samples (Harris et al. 1994). These libraries were sequenced on the Illumina Nextseq platform in high output mode with 75 cycles at the Biomolecular Resource Facility at The Australian National University. Illumina libraries were multiplexed in different ratios to account for the pure fungal reads in the in vitro samples (c. 20 million reads) compared to the mixed

plant and fungal reads in the in planta samples (c. 110 million reads).

2.3 | RNA Reads Mapping, Genome Annotation and Differential Gene Expression Analysis

The quality of RNA sequencing raw reads was assessed using FastQC (v. 0.11.8) (Andrews 2010). Low quality reads were removed and adapter sequences trimmed using Trimmomatic v. 0.33 with the following settings: –phred33 ILLUMINACLIP:TruSeq3-SE.fa:2:30:10 SLIDINGWINDOW:4:15 MINLEN:50 (Bolger et al. 2014). Trimmed reads from all in vitro and in planta samples were then combined and mapped to the WAI453 genome assembly using STAR v. 2.7.2a with the following settings: –twopassMode Basic –alignIntronMin 10 –alignIntronMax 300 (Dobin et al. 2013). The mapped reads were assembled into transcripts using StringTie v. 2.0 stranded library –rf mode (Pertea et al. 2015). Gene model prediction for the WAI453 genome assembly was performed using two gene model prediction software, BRAKER v. 2.0 (Brůna et al. 2021) and CodingQuarry v. 2.0 (Testa et al. 2015). Annotation with CodingQuarry v. 2.0 was performed using the 'pathogen stranded mode' and assembled transcripts were used as evidence for gene model prediction. BRAKER v. 2.0 gene model annotation was performed with mapped RNA-seq reads as input and using the –fungus parameter for fungal-specific intron prediction. Only the longest isoform from each predicted gene model was retained in the BRAKER output. EVidenceModeler (EVM) v. 1.1.1 (Haas et al. 2008) was then used to consolidate predicted gene models from CodingQuarry and BRAKER into a final annotation. Conflicting gene models were resolved by assigning weightings to annotations produced by each software. Four different weighting combinations were tested: CodingQuarry:BRAKER = 10:1, 10:4, 10:7 and 10:10. CodingQuarry was weighted 10 for all combinations because it is designed to predict small fungal genes such as effectors (Testa et al. 2015). The final annotation of WAI453 used the following weighting: CodingQuarry:BRAKER = 10:4.

Earlgrey v. 5.1.0 (Baril et al. 2024) was used to annotate transposable elements in the *R. commune* WAI453 genome using ascomycota as the search term in the RepeatMasker pipeline. Repeat-induced point (RIP) mutation analysis was performed in the RIPper web-based tool (van Wyk et al. 2019). This tool was run with the following options: RIP genome analysis window size 1000, slide size 500, minimum composite 0.01, minimum product 1.1, maximum substrate 0.75 and composite index chain 7. AT-richness across the genome was also measured with OcculterCut v. 1.1.1 (Testa et al. 2016).

For differential gene expression (DGE) analysis, trimmed reads from each in vitro and in planta sample were individually mapped to the WAI453 genome using STAR v. 2.7.2a with the following parameters: –alignIntronMin 10 –alignIntronMax 300 and with the new genome annotation as input (Dobin et al. 2013). The mapped reads were assembled into transcripts using StringTie v. 2.0 with parameters –rf –e –B –G. Mapped reads overlapping fungal coding regions and read counts were then extracted using the Python script (prepDE.py) (Pertea et al. 2015). EdgeR v. 3.26.8 (Robinson et al. 2010) was subsequently used to perform DGE analysis. Any predicted gene with less than 3 counts per million (cpm) in more than three individual samples was discarded, and the trimmed mean of *M*-values (TMM) method was used in the normalisation process. The glmQLFit function, which uses generalised linear models (GLMs) with quasi-likelihood (QL) *F*-test to test any group of samples, was used to generate a gene expression dataset including their *p*-value and the false discovery rate (FDR) value, with the contrast = 1 × in planta −1 × in vitro applied to identify differentially expressed genes (DEGs). The DGE group was generated using the Benjamini–Hochberg adjusted FDR method (Benjamini and Hochberg 1995) with $p < 0.01$ and $\log_2$ fold change ($\log_2$FC) or more. Reads per kilobase per million mapped reads of each gene (RPKM) in each biological treatment were calculated with the rpkm function in the EdgeR library. The full code detailing all steps described above for the DGE analysis and RPKM calculation is available in Zenodo (DOI: 10.5281/zenodo.14871345).

2.4 | *NIP2* and *NLP* Genes Detection From Global Isolates, Haplotype Networks and Phylogenetic Tree

The presence of *NIP2* and *NLP* genes in Australia_New isolates were first assessed using BLAST+ v. 2.9.0+ (Camacho et al. 2009) using *NIP2* and *NLP* sequences as the query input. A custom Python script, BLASTtoGFF_multiple.py (DOI:10.5281/zenodo.14871345), was then used to parse them into a fasta file. The *NIP2* and *NLP* genes from other *R. commune* global isolates and related species were extracted following the procedure of Mohd-Assaad et al. (2019).

To generate the haplotype network for each *NIP2* and *NLP* gene, *NIP2* and *NLP* gene sequences were aligned in the Phylip format. Missing nucleotides in the alignment were denoted with an 'X'. The alignments were imported into PopART v. 1.7 (Leigh and Bryant 2015), which was used to generate a haplotype network for each *NIP2* and *NLP* gene using a minimum spanning network.

To generate a phylogenetic tree from NIP2 and NLP proteins present in the *R. commune* global isolates and related species, protein sequences were firstly aligned with the Geneious Alignment in Geneious Prime 2019.1.3 (Kearse et al. 2012) with the following settings: global alignment, blosum 62 cost matrix, gap open penalty 12, gap extension penalty 3, refinement iterations 2. The alignment was adjusted to ensure each cysteine was in the same position. The best fitting amino acid substitution model was identified by inputting the final protein alignment into IQTree v. 2.0 (Kalyaanamoorthy et al. 2017; Nguyen et al. 2015). A Bayesian phylogenetic tree was created using MrBayes v. 3.2.6 (Huelsenbeck and Ronquist 2001) with the following settings: WAG Rate Matrix, gamma rate variation, four gamma categories, 1,000,000 chain length, four heated chains, 0.2 heated chain temperature, 10,000 subsampling frequency, 100,000 burn-in lengths and 3246 random seed. A maximum-likelihood tree (ML) was also created with RAxML v. 8.2.11 (Stamatakis 2014) with the following settings: GAMMA WAG protein model, rapid bootstrapping and search for best-scoring ML tree algorithm, 10,000 bootstrap replicates and 1250 parsimony random seed. Finally, the appearance of the phylogenetic tree was polished using FigTree v. 1.4.4 (Rambaut 2018).

2.5 | RNA Isolation and qPCR of *NIP2* Genes

Barley cv. ND5883 leaves were inoculated with the WAI453 isolate as described above for the RNA-seq infection assays. Infected leaves were collected from different time points: at 0 (less than 1 h after inoculation), 3, 6, 9 and 12 dpi. Three biological replicates for each sample were used in this experiment. Total RNA was extracted from these samples using Quick-RNA Fungal/Bacteria Miniprep (Zymo Research) following the manufacturer's protocol. Genomic DNA contamination was degraded using TURBO DNase (Thermo Fisher). First-strand cDNA was synthesised using SuperScript IV reverse transcriptase (Invitrogen) following the manufacturer's recommendation. cDNA samples were used for quantitative PCR (qPCR). Reactions were performed with Fast SYBR Green Master Mix (ThermoFisher) in a ViiA 7 Real-Time PCR System, following the Fast SYBR Green Master Mix recommendations. For calculating the amplification efficiency, standard curves for each primer set were generated according to the method described by Gardiner et al. (2004). The mean normalised expression (MNE) was used to analyse the expression of *NIP2.1*, *NIP2.3* and *NIP2.6* relative to *β-tubulin* expression according to Muller et al. (2002). Primers used in this study are listed in Table S1.

2.6 | NIP2.1 Functional Studies

The NIP2.1 protein was produced in *Escherichia coli* using the CyDisCo system as previously described (Yu et al. 2022). Intact mass spectrometry (MS) was performed on untreated NIP2.1 and NIP2.1 protein that was reduced by incubating in 10 mM dithiothreitol for 45 min at 56°C with agitation. Both samples were diluted to 10 μM in 0.1% formic acid before being run on an Agilent UHPLC system with an Agilent C3 trap column (ZORBAX StableBond C3) and Orbitrap Fusion Tribrid mass spectrometer (Thermo Fisher Scientific) according to Yu et al. (2022). The data was analysed in Free Style v. 1.4 (Thermo Fisher Scientific) program with the mass range setting 500–2000 *m/z*. Circular dichroism (CD) spectroscopy was carried out to confirm purified NIP2.1 protein contained secondary structure consistent with disulphide-bonded proteins. To do this, 10 μM of NIP2.1 protein diluted in 20 mM sodium phosphate pH 8 was analysed using a Chirascan spectrometer (Applied Photophysics Ltd) with a wavelength range from 200 to 260 nm and 0.5 nm wavelength increments. A scanning speed of 50 nm/min with three accumulations was used. The data were corrected with buffer control, averaged and visualised in the CAPITO web server with a data smoothing setting (Wiedemann et al. 2013).

To test the in planta activity of the purified protein, 10 μM or 160 μM of NIP2.1 was infiltrated with a 1 mL needleless syringe into the first leaf of 9-day-old barley cultivar Atlas 46 (*Rrs1* and *Rrs2*), Atlas (*Rrs2*) and ND5883 (no known major scald resistance genes). Infiltrated plants were incubated for 9 days in the growth chamber, as described above.

2.7 | NIP2 Structure Prediction

Structures of NIP2.1, NIP2.3 and NIP2.6 proteins (without their signal peptides) were predicted using Google DeepMind's AlphaFold colab notebook using default settings (https://colab.research.google.com/github/sokrypton/ColabFold/blob/main/AlphaFold2.ipynb) (Mirdita et al. 2022). To investigate potential structure-informed biological functions, proteins with a similar structure to the predicted structure of NIP2.1 were searched for using the Foldseek database in TM-align mode (van Kempen et al. 2023) and the DALI server (Holm and Rosenstrom 2010). The predicted NIP2.1 structure was aligned with other structurally similar proteins in the pairwise alignment mode in the DALI server (Holm and Rosenstrom 2010). The predicted structures and structural alignments were visualised using PyMOL (PyMOL Molecular Graphics System, v. 2.5.3; Schrödinger LLC).

3 | Results

3.1 | Pathotyping *R. commune* Isolate WAI453

A new collection of 72 *R. commune* isolates was isolated from infected leaves from different fields in NSW, Australia between 2013 and 2018. The virulence of WAI453 was tested against 26 barley cultivars with different known resistance genes or quantitative trait loci (QTLs) in two glasshouse seedling stage studies. This isolate was virulent on 10 out of 26 barley cultivars tested (Table 2). The 10 barley cultivars were heavily infected and categorised as susceptible and moderately susceptible–susceptible. Eight of these cultivars did not have any known scald resistance genes or QTLs. Atlas 46, Fathom, ICARDA 4 and Turk were the most resistant cultivars to the *R. commune* isolate WAI453 in this study. Atlas 46 and Turk carry the *Rrs1* (*Rh3*) gene, suggesting *R. commune* WAI453 carries the *NIP1* gene (Hahn et al. 1993). The *R. commune* isolate WAI453 also regularly produced conidia in vitro on lima bean agar plates in comparison to other isolates (data not shown). Given its amenability to in vitro growth and pathogenicity profile, WAI453 was used as source material for long-read genome sequencing to generate a high-quality reference assembly for an Australian *R. commune* isolate.

3.2 | Generating a Highly Contiguous Genome Assembly and Annotation for *R. commune* WAI453

To generate a chromosome-scale genome assembly, HMW genomic DNA of *R. commune* WAI453 was sequenced with PacBio Sequel using two SMRT cells, yielding 13.4 Gb of reads (Table S2). The resulting WAI453 assembly contained 23 contigs, of which 20 were nuclear DNA, one contig was mitochondrial DNA and two contigs contained solely ribosomal repeats (Figure 1A). The 20 nuclear contigs had a total length of 57.76 Mb and the genome N50 was 3.7 Mb (Table 3). Eleven contigs contained telomeric repeats on at least one end, and two contigs had telomeres at both ends, indicating two full chromosomes were obtained in this assembly. The number of contigs obtained was comparable with the number of predicted chromosomes of this fungus, which ranged from 13 to 16 (von Felten et al. 2011). Compared to the previously published *R. commune* reference UK7, the WAI453 genome assembly was 1.04% longer and contained 24× fewer contigs, indicating a significant improvement in the assembly contiguity for this species (Table 3; Penselin et al. 2016). Genome completeness

TABLE 2 | Disease resistance rating of different barley cultivars infected with *Rhynchosporium commune* WAI453.

Cultivar	Pedigree	Consensus seedling scald rating	Known resistance gene or QTL
AB240	CPI-109853 (*H. spontaneum*)/4*Clipper	MR	QTL on 3H
AB6	CPI-71283 (*H. spontaneum*)/4*Clipper	MR	*Rrs13*
Atlas	Landrace	MR	*Rrs2*
Atlas 46	Hanna/Atlas//Turk/Atlas	R-MR	*Rrs1* (*Rh3*) and *Rrs2*
Bass	WABAR2023/Alexis	MS-S	
Baudin	Stirling/Franklin	S	
Chieftain	Brittania/Prisma	MS-S	*Rrs1* (*Rh4*)
Fathom	JE-013D-020/WI-3806-1	R-MR	
Flinders	Baudin/Cooper	S	
Franklin	Shannon/Triumph	MS-S	APR on 3H at *Rrs1* position
Gairdner	Onslow//Shannon/Triumph	MS-S	*Rrs2*
GrangeR	Braemar/Adonis	MS	
Hindmarsh	Dash//O'Connor/WI-2723	MR	QTL on 3H at *Rrs1* position
ICARDA 4	Arar/Lignee 527	R-MR	QTL on 3H at *Rrs1* position
ICARDA 9	CI-07117-9/Deir Alla 106//Badia/3/Arar	MS-S	QTL on 3H at *Rrs1* position
Keel	CPI-18197/Clipper//Mari/CM67	MS	QTL on 3H and 6H
La Trobe	Dash//O'Connor/WI-2723	MR	QTL on 3H at *Rrs1* position
Litmus	WB229/2*Baudin//WABAR2238	S	
Maritime	Dampier//A14/3/Clipper/M11/5/Dampier//A14/4/Dampier//Prior/Ymer/3/Union	S	
Skiff	Abed Deba/3/Proctor/CI-3576//CPI-18197/Beka/4/Clipper/Diamant//Proctor/CI-3576	MR	*Rh*(*Skiff*)
Sloop	WI2468/Norbert//Golden Promise/WI2395/3/Schooner	S	
Tantangara	AB6/Skiff	MR	*Rrs13* and *Rh*(*Skiff*)
Turk	Landrace	R-MR	*Rrs1* (*Rh3*) and *Rh5*
Westminster	NSL 97-5547/Barke	MS	
Wimmera	VB0432	S	
Yerong	M22/Malebo	MR	QTL on 3H at *Rrs1* position

Abbreviations: QTL, quantitative trait locus. Scald ratings: R-MR, resistant-moderately resistant; MR, moderately resistant; MS, moderately susceptible; MS-S, moderately susceptible-susceptible; S, susceptible.

was assessed with the Benchmarking Universal Single-Copy Orthologs (BUSCO) tool (Simao et al. 2015). Among the 1315 orthologues present in the BUSCO Ascomycete set, 1299 (98.7%) were present in single copy in the WAI453 assembly (Figure S1).

The WAI453 genome was also assessed for the presence of transposable elements (TEs) using Earlgrey v. 5.1.0 (Baril et al. 2024). Approximately 31.81% of the *R. commune* WAI453 genome was predicted to consist of TEs, with about 25% classified as long terminal repeats (LTRs; Figure 1B). The genome was analysed for repeat-induced point (RIP) mutations, a genome defence mechanism observed in filamentous ascomycetes. This pathway is hypothesised to have evolved to limit the spread of TEs within the genome. During meiosis, RIP induces C-to-T and G-to-A mutations in repetitive sequences through an unknown mechanism. This process leads to AT-rich regions in the genome that contain few annotated genes (Clutterbuck 2011; Selker 2002). Approximately 30.58% of the *R. commune* WAI453 genome was affected by RIP mutations (Table 3).

A genome annotation for this new assembly was also generated using RNA-seq reads obtained from the third leaves of barley (cv. ND5883) 8 dpi and from an 8-day-old in vitro

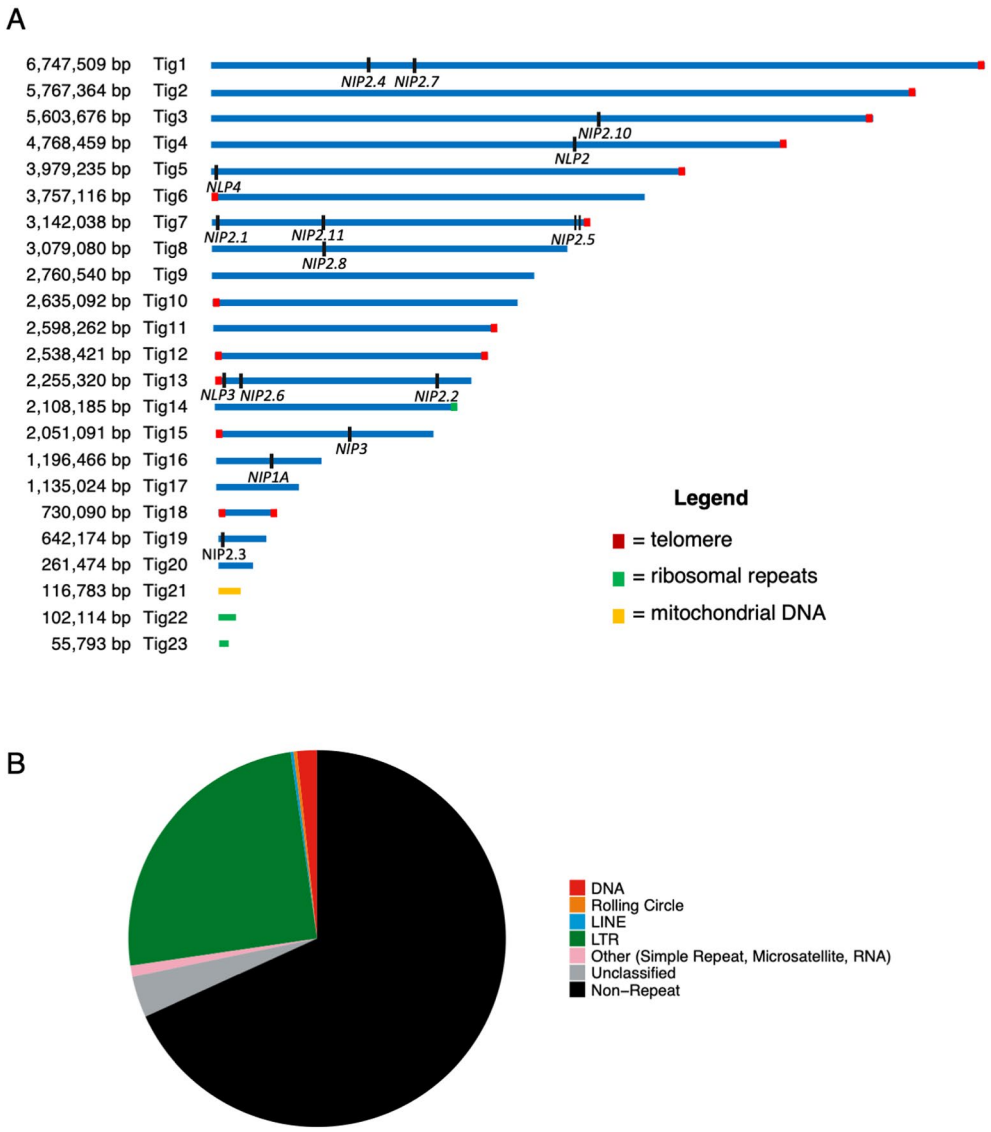

FIGURE 1 | (A) A schematic representation of the *Rhynchosporium commune* WAI453 de novo assembly showing all 23 contigs obtained. Nuclear chromosomes are shown as blue lines, whereas mitochondrial and rRNA repeat-containing contigs are coloured yellow and green, respectively. Contigs that contain telomeric repeats are noted with red boxes. The locations of *NIP1*, *NIP3*, *NIP2* and *NLP* genes in the *R. commune* WAI453 genome assembly are indicated with small black dashes. (B) Summary of different type of transposable elements present in the *R. commune* WAI453 genome detected by Earlgrey v. 5.1.0 (Baril et al. 2024). [Colour figure can be viewed at wileyonlinelibrary.com]

culture. The final annotation (EVidenceModeler with CodingQuarry:BRAKER = 10:4) contained 13,726 predicted genes and more than 97% of the Ascomycete BUSCO gene set was present (Tables 3 and S3, Figure S2). Approximately 9669 predicted proteins were small proteins (< 500 amino acids in size), and among these, 445 were predicted as secreted effectors containing a signal peptide (Figure S3, Table 3). The new annotation was also quality assessed by manually inspecting the annotation for each of the known *NIP2* and *NLP* effector genes. Most of the *NIP2* and *NLP* genes contain an intron in the 3′ UTR immediately following the stop codon. Using the RNA-seq data mapped to the WAI453 assembly, the presence of this 3′-UTR-intron was confirmed in the annotation of all *NIP2* and *NLP* genes (Figure S4A) with one exception in *NIP2.2* (Figure S4B). *NIP2.2* is the only paralogue that contains an intron in the protein coding sequence, which results in a slight shift in the total length of the protein. This paralogue is also the only *NIP2* that has a C-terminal extension region after the final cysteine, which was reported previously by Penselin et al. (2016).

BLASTn was used to identify the presence and location of all *NIP* and *NLP* genes, and the new annotation was cross-referenced with the published sequences for all named effectors. These analyses showed WAI453 carried *NIP1A* but not the paralogue *NIP1B*. WAI453 also carried 10 *NIP2* genes, missing only *NIP2.9* (Figure 1). In WAI453, three *NIP2* paralogues, *NIP2.5*, *NIP2.10* and *NLP2*, were determined to be pseudogenes, where *NLP2* had a single mutation in the start codon, *NIP2.10* had an 11 bp insertion introducing a premature stop codon, and the *NIP2.5* gene was separated into two fragments due to an approximately 3.2 kb insertion of a transposable element (Figure S5, Table S4). Among the *NLP* genes, *NLP2* and *NLP3* were found in this isolate, plus one newly

TABLE 3 | Comparison of *Rhynchosporium commune* WAI453 and *R. commune* UK7 genome assemblies.

Parameter	WAI453 (PacBio long-read sequencing)	UK7 (Illumina short-read sequencing)[a]
Coverage	232×	267×
Genome size	57.76 Mb	55.59 Mb
Contigs	20	481
Scaffolds	—	163
N50 contig	3757 kb	49.6 kb
N50 scaffold	—	800.5 kb
No. of predicted genes	13,726[b]	12,211
No. of predicted effectors with signal peptide[c]	445	359
Coding regions	17,158,241 bp	n.d.
AT-rich region[d]	30.5%	29.6%
RIP affected region[e]	30.58%	n.d.

[a]Penselin et al. (2016).
[b]Obtained after *R. commune* WAI453 genome annotation was performed.
[c]Analysed by SignalP 6.0 followed by EffectorP 3.0.
[d]Analysed by OcculterCut v1.1 (Testa et al. 2016).
[e]RIP, repeat-induced point mutation, analysed by The RIPper.

described *NLP*, now named *NLP4* (Figure 1). *NLP4* has the same characteristics as other described *NLP* genes, namely the six conserved cysteine residues and the 3′ UTR intron that are also shared with the *NIP2* genes. Together, this assembly and annotation gave us a comprehensive view of the entire *NIP2* and *NLP* gene family, which we used for further population genetic and functional analyses.

3.3 | Exploring the Presence of *NIP2* and *NLP* Paralogues in a Global Population and Related Species

To comprehensively explore the diversity of all *NIP2* and *NLP* paralogues, we used BLASTn to extract these genes from a global population collection of de novo assemblies, analysed previously for the diversity of *NIP1* (Mohd-Assaad et al. 2019; Table 1). We also added 72 new Australian *R. commune* isolates, including WAI453, to this dataset. These results showed that, with the exception of *NIP2.9*, most *NIP2* genes were largely present in different populations from around the world. *NIP2.9* was the only paralogue absent in 86.32% of all isolates globally. The Ethiopian population stood out from other populations as no isolates were found to carry *NIP2.6*, *NIP2.9* or *NIP2.10*, and only partial fragments of *NIP2.11* were identified. This indicates this population has undergone selective loss of these effectors when compared to other regions in the world. No other strong trends were observed that differentiated populations based on the presence or absence of these effectors.

Looking further at individual genes, the number of partial gene sequences obtained for *NIP2.5*, *NIP2.10*, *NIP2.11* and *NLP2* were much higher when compared to other paralogues (Figures 2A and S6). In particular, *NIP2.10* and *NLP2* had a high proportion (> 57%) of isolates carrying haplotypes with a premature stop codon (Figure S6). In contrast, all *R. commune* isolates in the global population had the complete *NIP2.4* and *NIP2.7* genes, while the *NIP2.3*, *NIP2.8* and *NLP3* genes were present in 99.47% of isolates (Figure 2A). The majority of the *R. commune* isolates in the global population also carried complete *NIP2.1* (95.79%), *NIP2.2* (94.74) and *NLP4* genes (97.37%). *NIP2.3* was the most highly conserved effector, with a single nucleotide haplotype found in all 189 isolates that had a complete *NIP2.3* gene (Figure S6), whereas *NIP2.1*, proposed to have necrosis activity, had the highest number of nucleotide haplotypes ($N = 11$) when compared to all other paralogues (Figure S6).

The presence of *NIP2* and *NLP* genes was also assessed in the two sister species, *R. agropyri* and *R. secalis*, as well as in the more distantly related *R. orthosporum* (Mohd-Assaad et al. 2019). All *R. agropyri* and *R. secalis* isolates had either complete or partial copies of *NIP2.2–5*, *NIP2.7–10*, *NLP3* and *NLP4* (Figure 2B). On the other hand, *NIP2.1* and *NIP2.6* were only present in *R. commune*. The most distantly related species, *R. orthosporum*, did not carry any of the 11 *NIP2* paralogues and only partial sequences of *NLP2* and *NLP3* in one out of four sequenced isolates. To better understand the evolution of this gene family within the species complex, a phylogenetic tree was constructed using all complete NIP2 and NLP proteins from *R. commune* and its sister species. The amino acid alignment of these NIP2 and NLP protein sequences showed the six conserved cysteine residues, while only NIP2 sequences, but not NLP sequences, had the CRS domain in the 66–68 residues in the alignment (Figure S7). In this phylogenetic tree, each numbered NIP2 and NLP paralogue grouped together with its sister species, indicating that gene duplication occurred before speciation (Figure 3). Given the absence of all *NIP2* genes in *R. orthosporum* but the presence of *NLP*

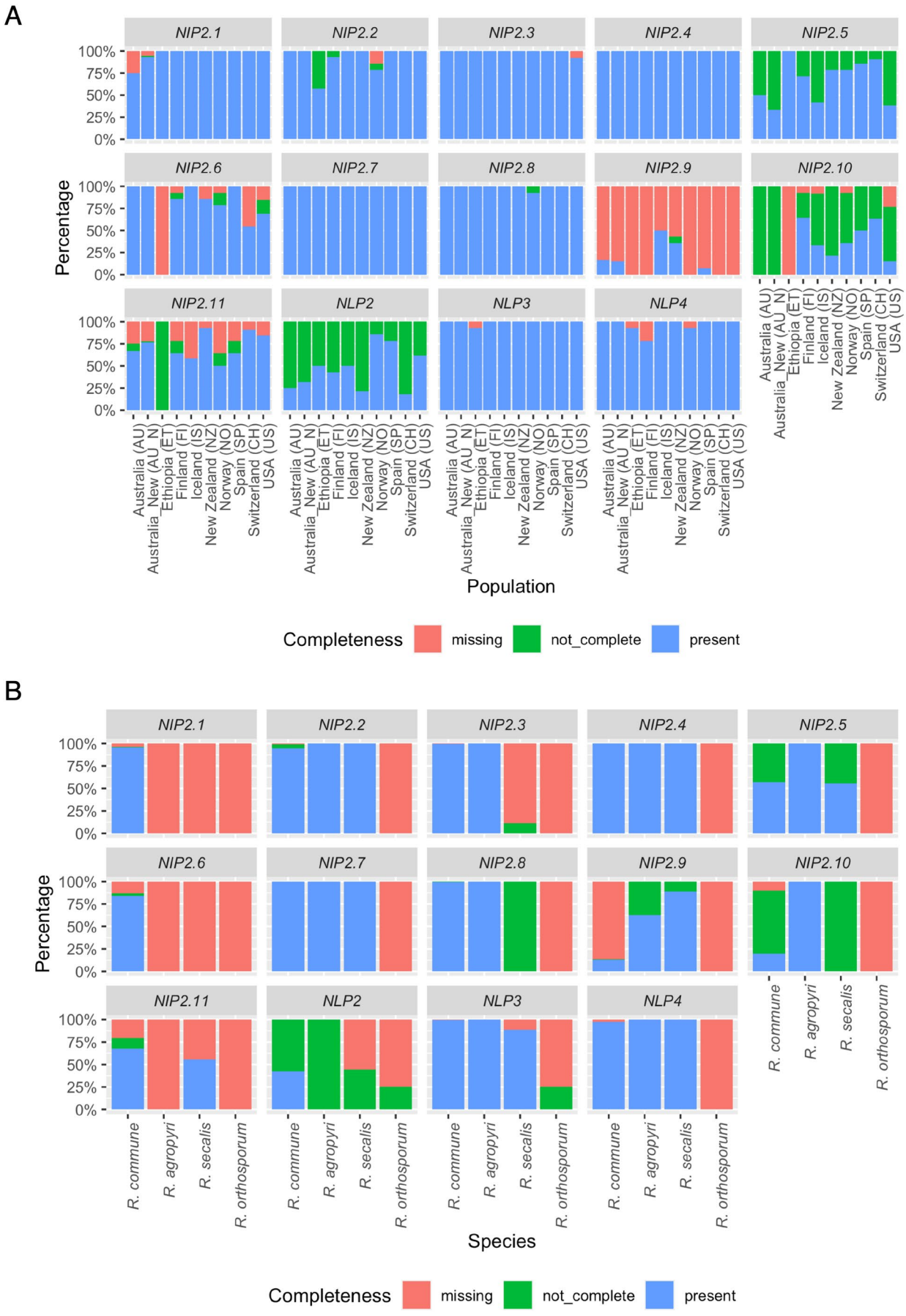

FIGURE 2 | Legend on next page.

FIGURE 2 | The presence-absence polymorphism of all *NIP2* and *NLP* genes in (A) global *Rhynchosporium commune* isolates, and (B) *R. commune* and three *R. commune* sister species. The presence of these genes is categorised into three groups, namely, present—isolate had a complete gene; not_complete—isolate only had some parts of the gene or had a premature stop codon inside the gene; and missing—isolate did not have the gene. [Colour figure can be viewed at wileyonlinelibrary.com]

gene fragments, it appears that the *NIP2* gene expansion occurred after the separation of the BCG species from the CCG species.

3.4 | *NIP2* and *NLP* Genes Are Upregulated During In Planta Growth

Our global screen indicated that most of the *NIP2* and *NLP* genes are present in *R. commune* global isolates and its sister species. However, there were distinct differences in sequence conservation between some paralogues (*NIP2.3* only one sequence haplotype globally) compared to paralogues that appear to be pseudogenes in a large number of isolates (*NIP2.5*, *NIP2.10* and *NLP2*). To further analyse how important these genes are for *R. commune* during infection, the expression of these genes in WAI453 was compared between 8 dpi-infected barley (in planta, IP samples) and 8-day-old in vitro culture (IV samples). A multidimensional scaling (MDS) plot was created from total aligned reads of all samples to compare the overall transcriptome profile of in vitro versus in planta samples (Figure 4A). This analysis showed all biological replicates from each group were tightly clustered, indicating a similar expression profile between the three biological replicates for each treatment. This analysis also showed, as expected, a clear separation between both growth conditions (Figure 4A). Differential gene expression analysis showed there were 1061 upregulated genes in planta (FDR 5%, $p < 0.01$), while only 418 genes were downregulated (Figure 4B). The expression of *NIP2* and *NLP* genes was then analysed from the DGE dataset. From 10 fully coding *NIP2* and *NLP* genes present in the WAI453 genome, we found seven were significantly upregulated during in planta infection, ranging from 2.08 to 6.93 $\log_2$FC (Table 4). Neither *NIP2.8* nor *NIP2.11* were expressed under the growth conditions tested in this study. The expression of *NIP2.2*, *NIP2.3*, *NIP2.4*, *NIP2.6* and *NIP2.7* was low during in vitro growth (< 35 RPKM), but was significantly induced in planta (90.86–324.07 RPKM; Table 4). In contrast, *NIP2.1* and *NLP3* were highly expressed in both growth conditions. *NLP3* had the highest expression level during in planta growth with almost 5000 RPKM, while its in vitro expression peaked at 115 RPKM. *NIP2.1* was not significantly differentially expressed (1.87 $\log_2$FC), but this gene was the second most highly expressed during the onset of necrosis, with more than 800 RPKM in planta and 219 RPKM in vitro (Table 4). The newly described *NLP4* was significantly differentially expressed between the two growth conditions, but overall very lowly expressed when compared to the other paralogues.

The DGE analysis was only performed at a single time point in planta (8 dpi), which did not give information regarding the trajectory of the expression of each of the *NIP2* genes throughout infection. Therefore, we performed qPCR on the *NIP2* genes at 0, 3, 6, 9 and 12 dpi to assess their expression during both the latent and necrotrophic phases of infection. In this experiment, the onset of necrosis was at 7 dpi. Given the large number of time points, this analysis was also limited to three phylogenetically distant *NIP2* genes, *NIP2.1*, *NIP2.3* and *NIP2.6* (Figure 3). The expression of *NIP2.1* was significantly higher than the expression of *NIP2.3* or *NIP2.6* at all time points tested, including the 0 dpi time point (Figure 4C). The gene expression of these three genes at 0 dpi was similar to what we observed in the RNA-seq analysis with in vitro samples where *NIP2.3* and *NIP2.6* were not expressed or lowly expressed but the *NIP2.1* expression reached 219 RPKM (Table 4). Over the course of these five time points, all three *NIP2* genes were most highly expressed during asymptomatic growth (3 dpi) and immediately prior to the onset of necrosis (6 dpi) (Figure 4C). *NIP2.1*, *NIP2.3* and *NIP2.6* were downregulated during the later stages of infection (after 9 dpi) (Figure 4C). Peak expression of *NIP2.1* was observed at the early stage of infection, which raises the question of whether or not *NIP2.1* has a function in inducing plant cell death.

3.5 | NIP2.1 Protein and Necrosis-Inducing Ability in Barley

NIP2 was originally described as one of three necrosis-inducing peptides (NIP1, 2 and 3) isolated from *R. commune* culture filtrates (Wevelsiep et al. 1991). According to Wevelsiep and colleagues, NIP2 represented a 6.8 kDa non-glycosylated secreted protein. The protein was identified in culture filtrates in all seven *R. commune* races tested. NIP2 protein purified from culture filtrate of the US238.1 strain caused necrosis at protein concentrations down to about 50 μg/mL (7 μM) in barley cultivars Atlas and Atlas 46. In a subsequent study, Kirsten et al. (2012) cloned the apparent NIP2 protein using *N*-terminal sequence data, referencing Wevelsiep et al. (1991), although these sequencing data were not reported in that study. The *NIP2* gene was subsequently cloned using a PCR walking strategy, with the cloned gene encoding a 93 amino-acid mature protein (without signal peptide) with a molecular weight of about 10 kDa, as verified by MS, which differs from the original molecular weight of NIP2 (Kirsten et al. 2012). The discrepancies in the reported molecular weight of NIP2 have not been addressed.

While studies since Wevelsiep et al. (1991) have confirmed the necrosis activity of NIP1 (Fiegen and Knogge 2002), to the best of our knowledge, no independent study has confirmed the necrosis activity of NIP2, despite the reported difference in size of the protein between the two studies described above. To address this, we heterologously expressed NIP2.1 in *E. coli* SHuffle (Lobstein et al. 2016) with the CyDisCo (cytoplasmic disulfide bond formation in the *E. coli*) system (Hatahet et al. 2010; Matos et al. 2014; Yu et al. 2022). We have used this system to investigate other necrosis-inducing proteins including Tox1 and Tox3 from *Parastagonospora nodorum* (Outram et al. 2021; Zhang et al. 2016). The NIP2.1 protein was purified to homogeneity and underwent quality control experiments, including the use

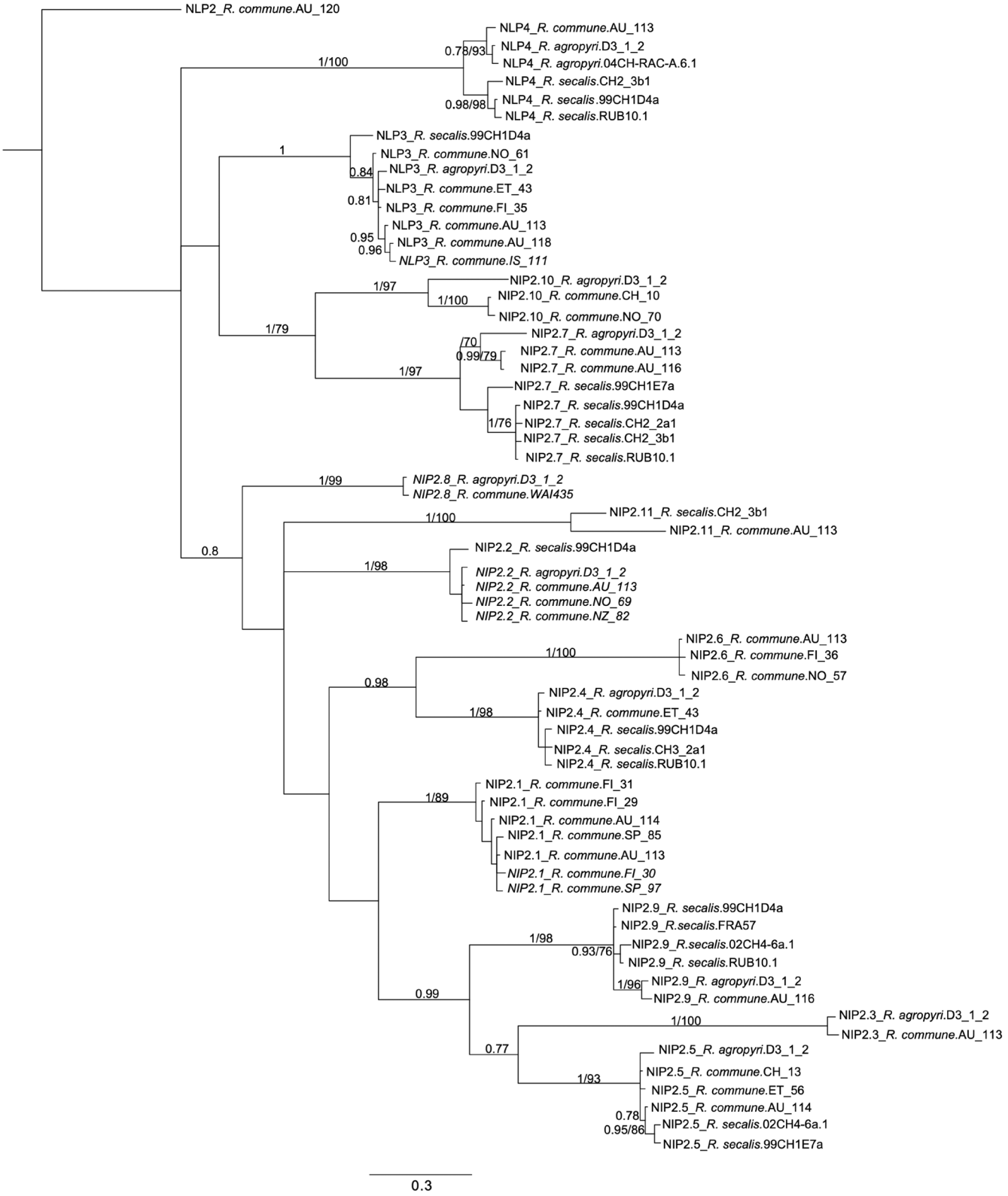

FIGURE 3 | Bayesian inference of phylogenetic tree of mature (without signal peptide) and complete (full length/without premature stop codon) NIP2 and NLP proteins from *Rhynchosporium commune* and its sister species. Numbers on the branches represent Bayesian posterior probabilities (≥0.70)/RA×ML bootstrap (≥70%) support values. Unique NIP2 sequences from *R. agropyri* 04CH-RAC-A.6.1 and *R. secalis* 02CH4-6a.1 were also used in this analysis (Penselin et al. 2016).

of circular dichroism to demonstrate the protein was correctly folded and intact protein MS to verify the formation of disulfide bonds, prior to infiltration experiments (Yu et al. 2022).

Pure, folded NIP2.1 protein was infiltrated into three different barley cultivars at concentrations of 10 or 160 μM, which were concentrations similar to and above that used by Wevelsiep

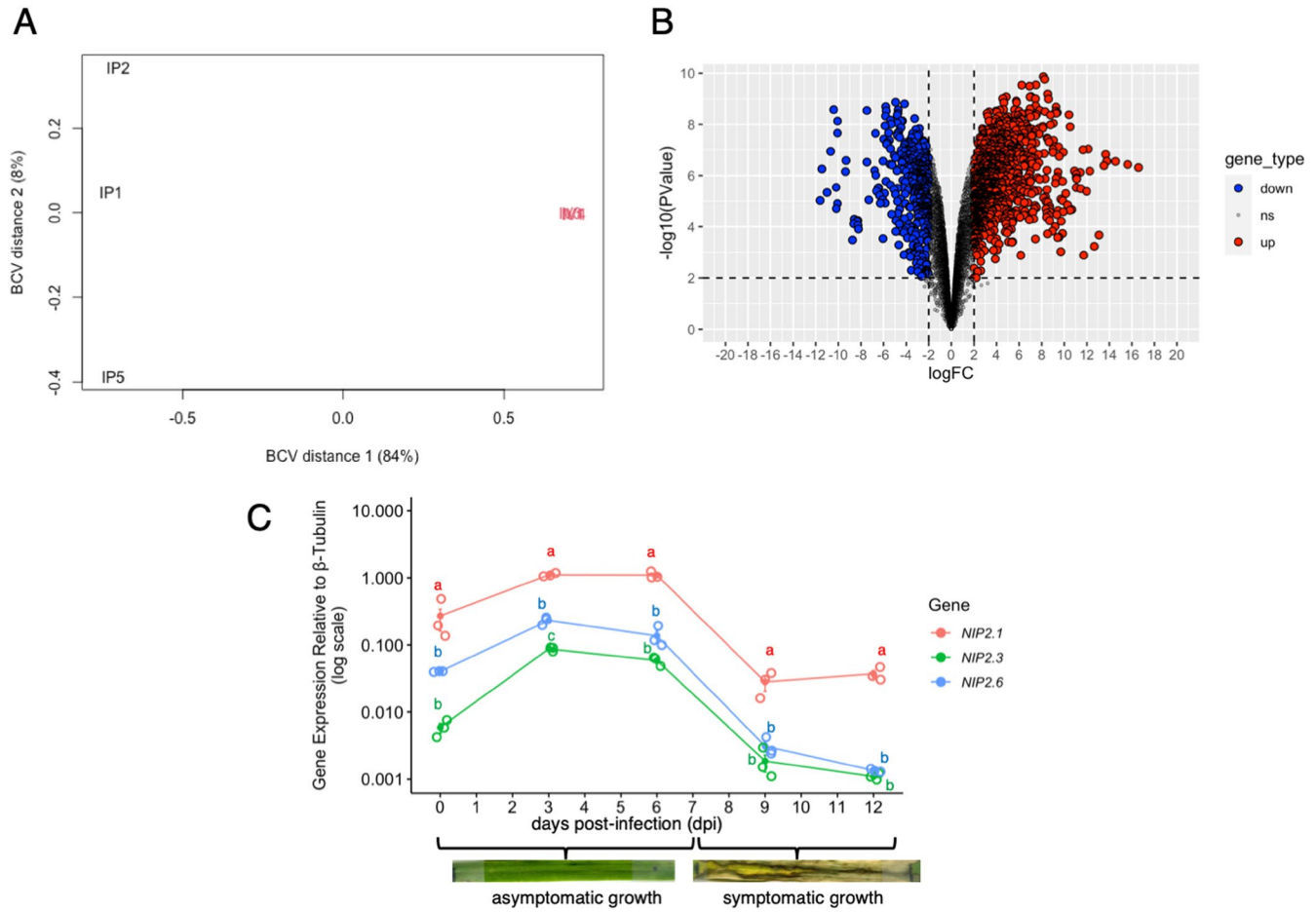

FIGURE 4 | (A) Multidimensional scaling (MDS) plot of the gene expression of *Rhynchosporium commune* WAI453 at 8 days post-inoculation (dpi) in planta on barley cv. ND5883 (labelled as IP) versus in vitro culture at 8 days (labelled as IV). The first biological coefficient of variation (BCV distance 1) separates IP and IV. (B) Volcano plot of the differentially expressed genes. Genes were considered differentially expressed if their $\log_2$ fold change ($\log_2$FC) was more than 2 or less than −2 and the *p*-value less than 0.01. There were 1061 upregulated genes ($\log_2\text{FC} \geq 2$), 418 downregulated genes ($\log_2\text{FC} \leq -2$) and 8144 not differentially expressed genes in 8 dpi-in planta growth. Red: upregulated genes. Blue: downregulated genes. (C) Gene expression of *NIP2.1*, *NIP2.3* and *NIP2.6* in *R. commune* WAI453 at different time points during infection, including asymptomatic and symptomatic growth. The necrotrophic switch was observed at 7 dpi. The expression of *NIP2* genes was monitored by reverse transcription-quantitative PCR (RT-qPCR) and normalised to *β-tubulin* expression. Standard error of the mean of three biological replicates (RNA from three separate leaves) is shown for each gene and time point. Data point for each replicate was shown using 'jitter' function in ggplot2. One-way ANOVA with least significant difference was performed to analyse the difference between *NIP2* genes expression in each time point. The same letter in each time point suggests they are not significantly different at $p < 0.05$. [Colour figure can be viewed at wileyonlinelibrary.com]

et al. (1991) (estimated to be about 7–20 μM). The three barley cultivars used were Atlas, which has the single dominant scald resistance gene *Rrs2*, Atlas 46, which has both *Rrs1* and *Rrs2* resistance genes, and ND5883, which has no known major scald resistance genes (Goodwin et al. 1990; Wallwork and Grcic 2011; Zhang et al. 2020). We did not observe necrosis on barley cultivars tested at any of the NIP2.1 concentrations at 9 dpi (Figure 5). Collectively, these data question the role of NIP2.1 as a necrosis-inducing protein.

Like many effectors, the sequence of NIP2 paralogues provides little insight concerning its potential function and role in pathogen virulence. Given the negative results reported above for induction of necrosis, we subsequently sought to use recent advances in AI-based protein structure prediction in the form of AlphaFold (Jumper et al. 2021; Mirdita et al. 2022) to predict the structure of NIP2 and investigate for structure-based similarities to other known effectors. The AlphaFold 2-generated NIP2.1 structure was predicted with high confidence (average predicted local distance difference test [pLDDT] score of c. 90 out of 100; Figure 6A). The predicted structure consists of a five-stranded β-sheet with a discontinuous α-helix connecting the β-1 and β-2 strands. The model includes three disulphide bonds, which we demonstrated experimentally (Yu et al. 2022). The AlphaFold2-generated NIP2.3 and NIP2.6 structures were also predicted with high confidence with pLDDT of approximately 89 and 86, respectively (Figure 6A). One of the disulphides was not predicted to form in these NIP2.3 and NIP2.6 models, but the cysteines localise to the same region in the NIP2.1 model and therefore probably form a disulphide as in the NIP2.1 predicted structure (Figure S8). This analysis suggests NIP2 paralogues potentially have a similar protein structure.

TABLE 4 | Transcript levels of *NIP2* and *NLP* genes in barley cv. ND5883 leaves infected with *Rhynchosporium commune* WAI453 at 8 days post-inoculation and in 8-day-old *R. commune* WAI453 in vitro culture.

Gene	Gene annotation	NCBI annotation	UK7 annotation	Log_2fold change	Relative expression in planta (RPKM)[a]	Relative expression in vitro (RPKM)[a]	Notes
NIP2.1	WAI453.tig_07.1.2	WAI453_007391	RC07_12002	1.87	801.70	219.65	
NIP2.2	WAI453.tig_13.417	WAI453_012037	RCO7_12003	5.85	212.78	3.66	
NIP2.3	WAI453.tig_19.4	WAI453_013593	RCO7_12004	6.93	324.07	2.64	
NIP2.4	WAI453.tig_01.338	WAI453_000338	RC07_12005 (incorrect gene prediction)	2.08	138.60	32.74	
NIP2.5	Tig_07 (3,084,075–3,084,213 (WAI453.tig_07.615) and 3,087,420–3,087,605)	WAI453_008005	Gene was separated into two fragments in contig FJUW01000059.1				Gene was not functional (gene was separated into two fragments)
NIP2.6	WAI453.tig_13.34	WAI453_011654	RCO7_07118	4.83	197.11	6.93	
NIP2.7	WAI453.tig_01.478	WAI453_000478	RCO7_14085	3.10	90.86	10.66	
NIP2.8	WAI453.tig_08.164	WAI453_008174	RC07_00629 (incorrect gene prediction)		n.d.[b]	n.d.[b]	
NIP2.9			Gene absent				Gene absent
NIP2.10	Tig_03 (WAI453.tig_03.774)	WAI453_003806	Unpredicted (gene is located in the contig FJUW01000004.1)				Gene was not functional (11 bp insertion leading to premature stop codon)
NIP2.11	WAI453.tig_07.119	WAI453_007509	Gene absent		n.d.[b]	n.d.[b]	
NLP2	Tig_04 (2804755–2,805,083)		RC07_10229				Gene was not functional (single mutation in start codon)
NLP3	WAI453.tig_13.2	WAI453_011622	RCO7_11479 (incorrect gene prediction)	5.42	4955.40	115.62	
NLP4	WAI453.tig_05.2	WAI453_005575	RCO7_15186	4.03	27.60	1.66	

[a]Reads per kilobase per million mapped reads (RPKM) values are the averages from three biological replicates.
[b]Expression of these genes was not detected (n.d.) under these conditions.

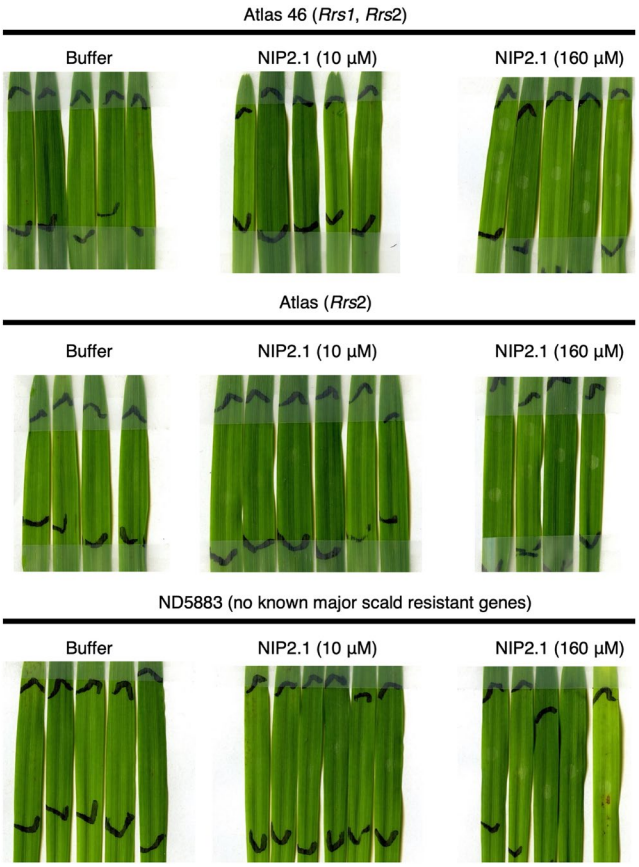

FIGURE 5 | Leaf infiltration assay of pure heterologously produced NIP2.1 protein. NIP2.1 protein at two concentrations (10 and 160 μM) was infiltrated into the first leaf of 9-day-old barley cultivar Atlas 46 (*Rrs1* and *Rrs2*), Atlas (*Rrs2*) and ND5883 (no known major scald resistance genes). Images were taken at 9 days post-infiltration. Black lines indicate the infiltration boundaries. [Colour figure can be viewed at wileyonlinelibrary.com]

Comparison of the NIP2.1 model with experimentally derived structures, using the Dali server (Holm and Rosenstrom 2010), provided little potential functional insights. A broader comparison of the predicted AlphaFold structural database, using the Foldseek server (van Kempen et al. 2023), suggested that NIP2.1 shares strong structural similarities with numerous putative fungal effector proteins including those from *Rhynchosporium*, *Fusarium* and *Colletotrichum* species. Notably, NIP2.1 did share some structural homology with the *Fusarium oxysporum* secreted-in-xylem (SIX) effectors *SIX9* and *SIX11* (Yu et al. 2024) with template modelling (TM) scores ranging from 0.559 to 0.838. Superimposing the predicted NIP2.1 structure with either AlphaFold model of SIX9 or SIX11 structure showed their structures were similar with a root mean square deviation (RSMD) of 2.5 and 3.7, respectively (Figure 6B). Taken together, by combining functional analysis and computational studies, our results suggest that the NIP2 protein, at least under the conditions used in our assays, does not induce necrosis on barley leaves.

4 | Discussion

Here, we described the presence and diversity of the *NIP2* and *NLP* genes across the *Rhynchosporium* spp. complex. This work shows that the majority of *NIP2* and *NLP* genes were present in the global population of *R. commune* and its sister species, *R. agropyri* and *R. secalis*, suggesting their importance for adaptability in different hosts and environments. Many *NIP2* genes were highly expressed during in planta growth, suggesting a role in facilitating infection. However, the NIP2.1 protein, following infiltration, did not induce necrosis on the barley leaves. Together these data suggest that *NIP2* genes do play a role in colonisation and infection, though the precise mechanism by which these genes facilitate infection remains unknown, as we provide strong evidence that NIP2.1 does not induce necrosis in barley as previously reported (Wevelsiep et al. 1991).

The duplication of *NIP2* and *NLP* genes was predicted to be an ancient duplication. This is supported by both the assembled genomic location of each paralogue and interspecific phylogenetic analyses conducted in this study. The de novo assembly generated for WAI453 is now the most contiguous and complete assembly available for this species. The total size of the assembly falls within the expected range of this species at approximately 57 Mb. When examining the distribution of the *NIP2* and *NLP* genes, there was very little evidence of clustering of these genes, with most copies found on unique contigs and/or several thousand kilobases apart from each other. The *NIP2/NLP* paralogues were highly variable in their distance to the nearest annotated transposon. In future work, it would be interesting to more closely examine the families of repeat elements found nearest to these genes to better understand if transposons have played a role in driving gene duplication. In previous work, Mohd-Assaad et al. (2019) noted that extra copies of *NIP1A* and *NIP1B* were located on smaller than average scaffolds and proposed that these highly identical copies may have been generated by tandem duplications during non-allelic homologous recombination. In WAI453, only a single copy of *NIP1A* was detected, so we were unable to explore this hypothesis further using our long-read sequencing data.

Each numbered paralogue grouped more closely with the same paralogue from a different species, indicating that these gene duplication events preceded speciation events. Of the 11 described *NIP2* genes, only *NIP2.6* was found in *R. commune* but not in its sister species, *R. secalis* or *R. agropyri*. While this gene forms a monophyletic group with *NIP2.4*, it remains unclear if this gene arose in *R. commune* alone or instead it has been lost in the other two sister species. Given the small sample size of available genomes for *R. secalis* ($N=9$) and *R. agropyri* ($N=8$), it is also likely this gene was simply not present in the available sequenced genomes. Similarly, no *NIP2* genes were detected in the four available *R. orthosporum* genomes. However, there was evidence of partial *NLP* gene sequences. Penselin et al. (2016) showed that *NIP2.1* was also present in other more distantly related *Rhynchosporium* species, including *R. orthosporum* and *R. lolii*, indicating that at least *NIP2.1* and/or *NLP* genes were present before the separation of the *Rhynchosporium* genus into the beaked conidia and cylindrical conidia groups. This indicates that the origins of the *NIP2* gene family trace back to an early evolutionary stage of this genus.

In pathogenic fungi, gene duplication and subsequent sequence divergence could lead to neofunctionalisation of those duplicated genes (Seong and Krasileva 2023; Shen et al. 2013). For example, the *Ustilago maydis* effectors *Tay1* and *Mer1* share 31%

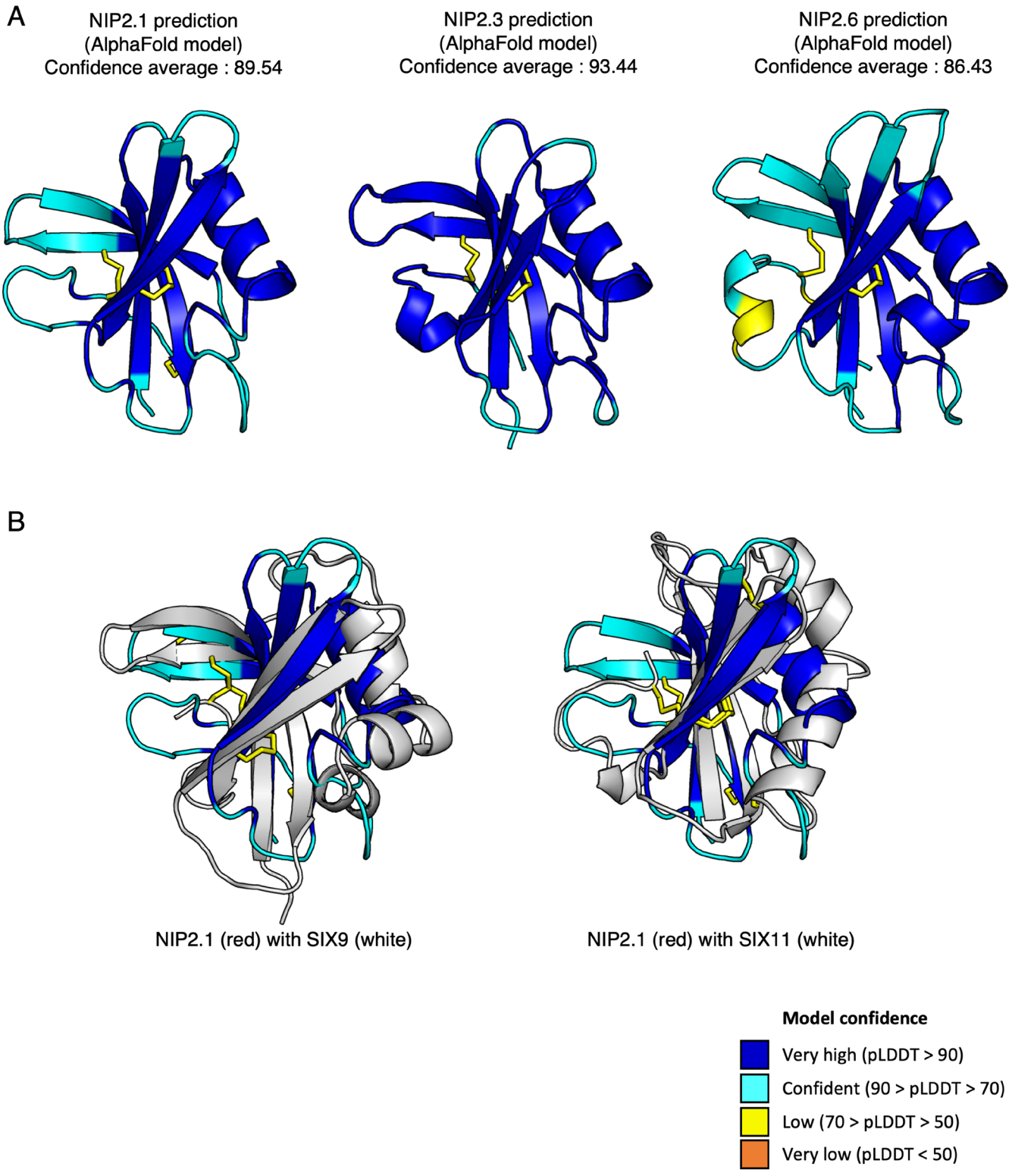

FIGURE 6 | (A) Structural prediction of mature (without signal peptide) NIP2.1, NIP2.3 and NIP2.6 proteins generated by AlphaFold 2. Each residue of each protein was coloured based on predicted local distance difference test (pLDDT) confidence score of AlphaFold 2 prediction. The predicted disulphide bridges are visualised as yellow sticks. (B) NIP2.1 predicted structure aligned with AlphaFold models of family 3 SIX effectors in white (Yu et al. 2024). SIX9 (left) and SIX11 (right) superimposed with a root mean square deviation (RSMD) of 2.5 and 3.7, respectively. [Colour figure can be viewed at wileyonlinelibrary.com]

protein sequence identity and have comparable functions to suppress the reactive oxygen species (ROS) burst but have different host targets (Navarrete et al. 2021). Tay1 acts in the cytoplasm while Mer1 acts in the nucleus, suggesting they have a different mode of action. Another example of gene duplication leading to neofunctionalisation is the expanded crinkling and necrosis inducing proteins (CRN) of *Phytophthora sojae*, which have less than 50% sequence similarity between half of those

gene members and display diverse biological functions such as the induction of apoptosis or a contrasting role in the suppression of programmed cell death (Shen et al. 2013). In addition, Avr4 of *Pseudocercospora fuligena* and its paralogue, Avr4-2, are another example of neofunctionalisation after gene duplication in pathogenic fungi. These proteins share 33% sequence identity but have different modes of interaction with the plant host (Chen et al. 2021). PfAvr4 binds chitin and protects the pathogen from chitinases, whereas PfAvr4-2 binds to de-esterified pectin of primary cell walls or the middle lamella of plant cells to disrupt cell wall formation (Chen et al. 2021). However, gene duplication can also lead to relaxed selection, where secondary copies simply become inactive (Lynch and Conery 2000; Seong and Krasileva 2023). There is some evidence of inactivation of some NIP2 paralogues, as over 57% of isolates found carrying *NIP2.10* and *NLP2* carry haplotypes that contain early stop codons. Similar to other paralogous effectors, the divergence of sequence from NIP2 and NLP proteins leads to the hypothesis that some of them might undergo neofunctionalisation or nonfunctionalisation, especially for those paralogues that have a different gene expression pattern or those paralogues that are mostly absent or present as incomplete proteins in the global population.

In this study, we found that five of the *NIP2* and *NLP* genes were found in more than 94.7% of the *R. commune* global population, and they were also highly expressed in WAI453 during infection with more than 2 $\log_2$FC compared to the in vitro growth. These findings suggest that the presence of multiple *NIP2* and *NLP* genes is important for *R. commune* during in planta growth. The presence of multiple copies of paralogues can be an important feature in fungal pathogen genomes to escape the plant's defence and maintain fungal virulence (Ridout et al. 2006). Only one paralogue of a fungal effector is usually recognised by a specific plant R protein. For example, AVRa7-1 (CSEP0059) is recognised by Mla7, while the paralogue CSEP0060 is not (Saur et al. 2019). Another example is the two AVR-Pik copies (AVR-PikD and AVR-PikF) present in some isolates of the rice blast fungus *Magnaporthe oryzae*, with only AVR-PikD being recognised by the Pik resistance protein (Longya et al. 2019). It could be advantageous for the pathogen to have multiple *NIP2* and *NLP* genes with comparable functions expressed simultaneously during in planta growth. If one of these paralogues was recognised by a barley R protein and the pathogen evolved to mutate or eliminate that specific *NIP2* gene to escape recognition, then other paralogues could still function to promote pathogen virulence without triggering plant defence responses.

However, despite the clear duplication of members within the NIP2 family, the actual role they play in facilitating disease is unclear. Wevelsiep et al. (1991) characterised a protein they identified as NIP2 from *R. commune* and provided evidence that this protein induced necrosis in barley. However, the sequence of the infiltrated protein from this work was not published, and the NIP2 sequence itself was not reported in the literature until it was identified by Kirsten et al. (2012). There is a small size difference between the 6.8 kDa protein reported as NIP2 by Wevelsiep et al. (1991) and the reported 10.03 kDa mature NIP2 sequence reported by Kirsten et al. (2012). This discrepancy suggests there may be a mismatch between the activity observed in the necrosis assay and the identified protein. Here, NIP2 was produced heterologously and infiltrated into barley at concentrations similar to that reported previously to cause necrosis (Wevelsiep et al. 1991). However, these infiltrations failed to induce any necrotic symptoms in barley leaves. We produced NIP2.1 in *E. coli* SHuffle with CyDisCo, which can be used to produce other active necrosis-inducing proteins from other pathogenic fungi. Such examples include the Tox proteins from *P. nodorum* that were shown to be highly active following heterologous expression and able to induce cell death (Yu et al. 2022). Extensive biochemical tests confirmed the purity and the correct folding of the heterologously expressed NIP2.1, suggesting it was an active protein (Yu et al. 2022). Our data demonstrate that the protein encoded by the published NIP2.1 sequences does not induce necrosis on barley leaves. Due to the time and expense of producing these effector proteins heterologously, we were unable to explore this activity in all the NIP2 paralogues in this study; however, given their high degree of structural similarity, we consider this unlikely.

The inability of NIP2.1 and its paralogues to elicit plant cell death on barley leaves is supported by another experiment conducted by Zaffarano et al. (2008) who analysed the ability of different *Rhynchosporium* species to infect barley leaves. *R. commune* was the only species of *Rhynchosporium* that could infect and produce visible symptoms on barley leaves, while other *Rhynchosporium* species isolated from rye and triticale (*R. secalis*) and *Agropyron repens* (*R. agropyri*) were unable to cause visible symptoms on inoculated barley leaves (Zaffarano et al. 2008, 2011). However, Penselin et al. (2016) did show that *R. secalis* and *R. agropyri* also possess the *NIP2.1* gene, suggesting that *NIP2.1* was not specific to *R. commune* for inducing necrosis on barley leaves. Our data also show that these two species carry most of the other *NIP2* paralogues. Collectively, and combined with our data, these studies cast doubt over the role of NIP2.1 (and potentially other NIP2 proteins) to induce cell death in barley. While negative, this result now enables future work to focus on other potential functions of this highly expressed effector gene family in facilitating disease.

In conclusion, our study revealed the diversity of *NIP2* and *NLP* genes in *R. commune* and its sister species, which likely originated from ancient duplications. RNA-sequencing and expression analyses consistently showed upregulation of these genes during the early stages of infection, suggesting their role in promoting infection, whilst functional studies demonstrated that NIP2.1 does not induce necrosis as previously reported. These findings enhance our understanding of paralogous effectors in *R. commune*.

Acknowledgements

We thank Haochen Wei for her technical assistance with the RNA-seq analysis and Arild Ranlym Arifin for his technical assistance with phylogenetic tree analysis. We acknowledge RSB plant services and NCRIS facility team and The ANU's Biomolecular Resource Facility for supporting our research. R.D. was supported by The Australian National University scholarships and The British Society for Plant Pathology (BSPP) COVID-19 support. Funding was provided by the Grains Research and Development Corporation under the National barley foliar pathogen variety improvement programme (DAQ00187).

Conflicts of Interest

The authors declare no conflicts of interest.

Data Availability Statement

Raw genome sequencing, raw RNA-Seq, genome assembly of WAI453 and the genome annotation of WAI453 are deposited at https://www.ncbi.nlm.nih.gov/genbank/ under NCBI project PRJNA910335. Genome assembly and genome annotation of WAI453 are also available in Zenodo (DOI:10.5281/zenodo.14871345). All raw genome sequencing of other Australia_New isolates is deposited under NCBI project PRJNA914478.

References

Andrews, S. 2010. "FastQC: A Quality Control Tool for High Throughput Sequence Data." https://www.bioinformatics.babraham.ac.uk/projects/fastqc/.

Avrova, A., and W. Knogge. 2012. "*Rhynchosporium commune*: A Persistent Threat to Barley Cultivation." *Molecular Plant Pathology* 13: 986–997.

Bankevich, A., S. Nurk, D. Antipov, et al. 2012. "SPAdes: A New Genome Assembly Algorithm and Its Applications to Single-Cell Sequencing." *Journal of Computational Biology* 19: 455–477.

Baril, T., J. Galbraith, and A. Hayward. 2024. "Earl Grey: A Fully Automated User-Friendly Transposable Element Annotation and Analysis Pipeline." *Molecular Biology and Evolution* 41: msae068.

Benjamini, Y., and Y. Hochberg. 1995. "Controlling the False Discovery Rate: A Practical and Powerful Approach to Multiple Testing." *Journal of the Royal Statistical Society: Series B: Methodological* 57: 289–300.

Bolger, A. M., M. Lohse, and B. Usadel. 2014. "Trimmomatic: A Flexible Trimmer for Illumina Sequence Data." *Bioinformatics* 30: 2114–2120.

Brown, J. S. 1985. "Pathogenic Variation Among Isolates of *Rhynchosporium secalis* From Cultivated Barley Growing in Victoria, Australia." *Euphytica* 34: 129–133.

Brůna, T., K. J. Hoff, A. Lomsadze, M. Stanke, and M. Borodovsky. 2021. "BRAKER2: Automatic Eukaryotic Genome Annotation With GeneMark-EP+ and AUGUSTUS Supported by a Protein Database." *NAR Genomics and Bioinformatics* 3: lqaa108.

Camacho, C., G. Coulouris, V. Avagyan, et al. 2009. "BLAST+: Architecture and Applications." *BMC Bioinformatics* 10: 421.

Chen, L. H., S. K. Kracun, K. S. Nissen, et al. 2021. "A Diverse Member of the Fungal Avr4 Effector Family Interacts With De-Esterified Pectin in Plant Cell Walls to Disrupt Their Integrity." *Science Advances* 7: eabe0809.

Clutterbuck, A. J. 2011. "Genomic Evidence of Repeat-Induced Point Mutation (RIP) in Filamentous Ascomycetes." *Fungal Genetics and Biology* 48: 306–326.

Darma, R., and M. McDonald. 2019. "High Molecular Weight DNA Extraction From Fungal Tissue for the Long Read PacBio Sequencing." *Protocols.io*. https://doi.org/10.17504/protocols.io.9g3h3yn.

Dobin, A., C. A. Davis, F. Schlesinger, et al. 2013. "STAR: Ultrafast Universal RNA-Seq Aligner." *Bioinformatics* 29: 15–21.

Fetch, T. G., and B. J. Steffenson. 1994. "Identification of *Cochliobolus sativus* Isolates Expressing Differential Virulence on Two-Row Barley Genotypes From North Dakota." *Canadian Journal of Plant Pathology* 16: 202–206.

Fiegen, M., and W. Knogge. 2002. "Amino Acid Alterations in Isoforms of the Effector Protein NIP1 From *Rhynchosporium secalis* Have Similar Effects on Its Avirulence- and Virulence-Associated Activities on Barley." *Physiological and Molecular Plant Pathology* 61: 299–302.

Gardiner, D. M., A. J. Cozijnsen, L. M. Wilson, M. S. Pedras, and B. J. Howlett. 2004. "The Sirodesmin Biosynthetic Gene Cluster of the Plant Pathogenic Fungus *Leptosphaeria maculans*." *Molecular Microbiology* 53: 1307–1318.

Goodwin, S. B. 2002. "The Barley Scald Pathogen *Rhynchosporium secalis* Is Closely Related to the Discomycetes *Tapesia* and *Pyrenopeziza*." *Mycological Research* 106: 645–654.

Goodwin, S. B., R. W. Allard, and R. K. Webster. 1990. "A Nomenclature for *Rhynchosporium secalis* Pathotypes." *Phytopathology* 80: 1330–1336.

Haas, B. J., S. L. Salzberg, W. Zhu, et al. 2008. "Automated Eukaryotic Gene Structure Annotation Using EVidenceModeler and the Program to Assemble Spliced Alignments." *Genome Biology* 9: R7.

Hahn, M., S. Jungling, and W. Knogge. 1993. "Cultivar-Specific Elicitation of Barley Defense Reactions by the Phytotoxic Peptide NIP1 From *Rhynchosporium secalis*." *Molecular Plant–Microbe Interactions* 6: 745–754.

Harris, E. H., J. E. Boynton, and N. W. Gillham. 1994. "Chloroplast Ribosomes and Protein Synthesis." *Microbiological Reviews* 58: 700–754.

Hatahet, F., V. D. Nguyen, K. E. H. Salo, and L. W. Ruddock. 2010. "Disruption of Reducing Pathways Is Not Essential for Efficient Disulfide Bond Formation in the Cytoplasm of *E. coli*." *Microbial Cell Factories* 9: 67.

Holm, L., and P. Rosenstrom. 2010. "Dali Server: Conservation Mapping in 3D." *Nucleic Acids Research* 38: W545–W549.

Huelsenbeck, J. P., and F. Ronquist. 2001. "MrBayes: Bayesian Inference of Phylogenetic Trees." *Bioinformatics* 17: 754–755.

Jumper, J., R. Evans, A. Pritzel, et al. 2021. "Highly Accurate Protein Structure Prediction With AlphaFold." *Nature* 596: 583–589.

Kalyaanamoorthy, S., B. Q. Minh, T. K. F. Wong, A. von Haeseler, and L. S. Jermiin. 2017. "ModelFinder: Fast Model Selection for Accurate Phylogenetic Estimates." *Nature Methods* 14: 587–589.

Kearse, M., R. Moir, A. Wilson, et al. 2012. "Geneious Basic: An Integrated and Extendable Desktop Software Platform for the Organization and Analysis of Sequence Data." *Bioinformatics* 28: 1647–1649.

King, K. M., J. S. West, P. C. Brunner, P. S. Dyer, and B. D. L. Fitt. 2013. "Evolutionary Relationships Between *Rhynchosporium lolii* sp. nov. and Other *Rhynchosporium* Species on Grasses." *PLoS One* 8: e72536.

Kirsten, S., A. Navarro-Quezada, D. Penselin, et al. 2012. "Necrosis-Inducing Proteins of *Rhynchosporium commune*, Effectors in Quantitative Disease Resistance." *Molecular Plant–Microbe Interactions* 25: 1314–1325.

Koren, S., B. P. Walenz, K. Berlin, J. R. Miller, N. H. Bergman, and A. M. Phillippy. 2017. "Canu: Scalable and Accurate Long-Read Assembly via Adaptive k-Mer Weighting and Repeat Separation." *Genome Research* 27: 722–736.

Leigh, J. W., and D. Bryant. 2015. "PopART: Full-Feature Software for Haplotype Network Construction." *Methods in Ecology and Evolution* 6: 1110–1116.

Linde, C. C., M. Zala, S. Ceccarelli, and B. A. McDonald. 2003. "Further Evidence for Sexual Reproduction in *Rhynchosporium secalis* Based on Distribution and Frequency of Mating-Type Alleles." *Fungal Genetics and Biology* 40: 115–125.

Linde, C. C., M. Zala, and B. A. McDonald. 2009. "Molecular Evidence for Recent Founder Populations and Human-Mediated Migration in the Barley Scald Pathogen *Rhynchosporium secalis*." *Molecular Phylogenetics and Evolution* 51: 454–464.

Lobstein, J., C. A. Emrich, C. Jeans, M. Faulkner, P. Riggs, and M. Berkmen. 2016. "Erratum to: SHuffle, a Novel *Escherichia coli* Protein Expression Strain Capable of Correctly Folding Disulfide Bonded Proteins in Its Cytoplasm." *Microbial Cell Factories* 15: 124.

Longya, A., C. Chaipanya, M. Franceschetti, J. H. R. Maidment, M. J. Banfield, and C. Jantasuriyarat. 2019. "Gene Duplication and Mutation in the Emergence of a Novel Aggressive Allele of the *AVR-Pik* Effector in the Rice Blast Fungus." *Molecular Plant–Microbe Interactions* 32: 740–749.

Lu, X., J. Miao, D. Shen, and D. Dou. 2022. "Proteinaceous Effector Discovery and Characterization in Plant Pathogenic *Colletotrichum* Fungi." *Frontiers in Microbiology* 13: 914035.

Lynch, M., and J. S. Conery. 2000. "The Evolutionary Fate and Consequences of Duplicate Genes." *Science* 290: 1151–1155.

Matos, C. F. R. O., C. Robinson, H. I. Alanen, et al. 2014. "Efficient Export of Prefolded, Disulfide-Bonded Recombinant Proteins to the Periplasm by the Tat Pathway in *Escherichia coli* CyDisCo Strains." *Biotechnology Progress* 30: 281–290.

McDermott, J. M., B. A. McDonald, R. W. Allard, and R. K. Webster. 1989. "Genetic Variability for Pathogenicity, Isozyme, Ribosomal DNA and Colony Color Variants in Populations of *Rhynchosporium secalis*." *Genetics* 122: 561–565.

McDonald, B. A., J. Zhan, and J. J. Burdon. 1999. "Genetic Structure of *Rhynchosporium secalis* in Australia." *Phytopathology* 89: 639–645.

McDonald, M. C., D. Ahren, S. Simpfendorfer, A. Milgate, and P. S. Solomon. 2018. "The Discovery of the Virulence Gene *ToxA* in the Wheat and Barley Pathogen *Bipolaris sorokiniana*." *Molecular Plant Pathology* 19: 432–439.

Mirdita, M., K. Schütze, Y. Moriwaki, L. Heo, S. Ovchinnikov, and M. Steinegger. 2022. "ColabFold: Making Protein Folding Accessible to all." *Nature Methods* 19: 679–682.

Mohd-Assaad, N., B. A. McDonald, and D. Croll. 2019. "The Emergence of the Multi-Species NIP1 Effector in *Rhynchosporium* Was Accompanied by High Rates of Gene Duplications and Losses." *Environmental Microbiology* 21: 2677–2695.

Muller, P. Y., H. Janovjak, A. R. Miserez, and Z. Dobbie. 2002. "Processing of Gene Expression Data Generated by Quantitative Real-Time RT-PCR." *BioTechniques* 32: 1372–1374.

Navarrete, F., N. Grujic, A. Stirnberg, et al. 2021. "The Pleiades Are a Cluster of Fungal Effectors That Inhibit Host Defenses." *PLoS Pathogens* 17: e1009641.

Nguyen, L. T., H. A. Schmidt, A. von Haeseler, and B. Q. Minh. 2015. "IQ-TREE: A Fast and Effective Stochastic Algorithm for Estimating Maximum-Likelihood Phylogenies." *Molecular Biology and Evolution* 32: 268–274.

Outram, M. A., Y. C. Sung, D. Yu, et al. 2021. "The Crystal Structure of SnTox3 From the Necrotrophic Fungus *Parastagonospora nodorum* Reveals a Unique Effector Fold and Provides Insight Into Snn3 Recognition and Pro-Domain Protease Processing of Fungal Effectors." *New Phytologist* 231: 2282–2296.

Paveley, N., B. Fitt, S. J. P. Oxley, et al. 2016. *The Barley Disease Management Guide*. Agriculture and Horticulture Development Board Cereals and Oilseeds.

Penselin, D., M. Munsterkotter, S. Kirsten, et al. 2016. "Comparative Genomics to Explore Phylogenetic Relationship, Cryptic Sexual Potential and Host Specificity of *Rhynchosporium* Species on Grasses." *BMC Genomics* 17: 953.

Pertea, M., G. M. Pertea, C. M. Antonescu, T. C. Chang, J. T. Mendell, and S. L. Salzberg. 2015. "StringTie Enables Improved Reconstruction of a Transcriptome From RNA-Seq Reads." *Nature Biotechnology* 33: 290–295.

Rambaut, A. 2018. *FigTree v1.4.4: Molecular Evolution, Phylogenetics and Epidemiology*. University of Edinburgh. https://tree.bio.ed.ac.uk/software/Figtree/.

Ridout, C. J., P. Skamnioti, O. Porritt, S. Sacristan, J. D. Jones, and J. K. Brown. 2006. "Multiple Avirulence Paralogues in Cereal Powdery Mildew Fungi May Contribute to Parasite Fitness and Defeat of Plant Resistance." *Plant Cell* 18: 2402–2414.

Robinson, M. D., D. J. McCarthy, and G. K. Smyth. 2010. "edgeR: A Bioconductor Package for Differential Expression Analysis of Digital Gene Expression Data." *Bioinformatics* 26: 139–140.

Salamati, S., J. Zhan, J. J. Burdon, and B. A. McDonald. 2000. "The Genetic Structure of Field Populations of *Rhynchosporium secalis* From Three Continents Suggests Moderate Gene Flow and Regular Recombination." *Phytopathology* 90: 901–908.

Saur, I. M., S. Bauer, B. Kracher, et al. 2019. "Multiple Pairs of Allelic MLA Immune Receptor-Powdery Mildew AVR_A Effectors Argue for a Direct Recognition Mechanism." *eLife* 8: e44471.

Selker, E. U. 2002. "Repeat-Induced Gene Silencing in Fungi." *Advances in Genetics* 46: 439–450.

Seong, K., and K. V. Krasileva. 2023. "Prediction of Effector Protein Structures From Fungal Phytopathogens Enables Evolutionary Analyses." *Nature Microbiology* 8: 174–187.

Shao, D., D. L. Smith, M. Kabbage, and M. G. Roth. 2021. "Effectors of Plant Necrotrophic Fungi." *Frontiers in Plant Science* 12: 687713.

Shen, D., T. Liu, W. Ye, et al. 2013. "Gene Duplication and Fragment Recombination Drive Functional Diversification of a Superfamily of Cytoplasmic Effectors in *Phytophthora sojae*." *PLoS One* 8: e70036.

Simao, F. A., R. M. Waterhouse, P. Ioannidis, E. V. Kriventseva, and E. M. Zdobnov. 2015. "BUSCO: Assessing Genome Assembly and Annotation Completeness With Single-Copy Orthologs." *Bioinformatics* 31: 3210–3212.

Skoropad, W. P. 1959. "Seed and Seedling Infection of Barley by *Rhynchosporium secalis*." *Phytopathology* 49: 623–626.

Stamatakis, A. 2014. "RAxML Version 8: A Tool for Phylogenetic Analysis and Post-Analysis of Large Phylogenies." *Bioinformatics* 30: 1312–1313.

Stefansson, T. S., B. A. McDonald, and Y. Willi. 2013. "Local Adaptation and Evolutionary Potential Along a Temperature Gradient in the Fungal Pathogen *Rhynchosporium commune*." *Evolutionary Applications* 6: 524–534.

Testa, A. C., J. K. Hane, S. R. Ellwood, and R. P. Oliver. 2015. "CodingQuarry: Highly Accurate Hidden Markov Model Gene Prediction in Fungal Genomes Using RNA-Seq Transcripts." *BMC Genomics* 16: 170.

Testa, A. C., R. P. Oliver, and J. K. Hane. 2016. "OcculterCut: A Comprehensive Survey of AT-Rich Regions in Fungal Genomes." *Genome Biology and Evolution* 8: 2044–2064.

van Kempen, M., S. S. Kim, C. Tumescheit, et al. 2023. "Fast and Accurate Protein Structure Search With Foldseek." *Nature Biotechnology* 42: 243–246.

van Wyk, S., C. H. Harrison, B. D. Wingfield, L. De Vos, N. A. van der Merwe, and E. T. Steenkamp. 2019. "The RIPper, a Web-Based Tool for Genome-Wide Quantification of Repeat-Induced Point (RIP) Mutations." *PeerJ* 7: e7447.

von Felten, A., P. L. Zaffarano, and B. A. McDonald. 2011. "Electrophoretic Karyotypes of *Rhynchosporium commune*, *R. secalis* and *R. agropyri*." *European Journal of Plant Pathology* 129: 529–537.

Wallwork, H., and M. Grcic. 2011. "The Use of Differential Isolates of *Rhynchosporium secalis* to Identify Resistance to Leaf Scald in Barley." *Australasian Plant Pathology* 40: 490–496.

Wevelsiep, L., K.-H. Kogel, and W. Knogge. 1991. "Purification and Characterization of Peptides From *Rhynchosporium secalis* Inducing Necrosis in Barley." *Physiological and Molecular Plant Pathology* 39: 471–482.

Wevelsiep, L., E. Rupping, and W. Knogge. 1993. "Stimulation of Barley Plasmalemma H^+-ATPase by Phytotoxic Peptides From the Fungal Pathogen *Rhynchosporium secalis*." *Plant Physiology* 101: 297–301.

Wiedemann, C., P. Bellstedt, and M. Görlach. 2013. "CAPITO—A Web Server-Based Analysis and Plotting Tool for Circular Dichroism Data." *Bioinformatics* 29: 1750–1757.

Yu, D. S., M. A. Outram, E. Crean, et al. 2022. "Optimised Production of Disulfide-Bonded Fungal Effectors in *E. coli* Using CyDisCo and FunCyDisCo Co-Expression Approaches." *Molecular Plant–Microbe Interactions* 35: 109–118.

Yu, D. S., M. A. Outram, A. Smith, et al. 2024. "The Structural Repertoire of *Fusarium oxysporum f.* sp. *lycopersici* Effectors Revealed by Experimental and Computational Studies." *eLife* 12: RP89280.

Zaffarano, P. L., B. A. McDonald, and C. C. Linde. 2008. "Rapid Speciation Following Recent Host Shifts in the Plant Pathogenic Fungus *Rhynchosporium*." *Evolution* 62: 1418–1436.

Zaffarano, P. L., B. A. McDonald, and C. C. Linde. 2011. "Two New Species of *Rhynchosporium*." *Mycologia* 103: 195–202.

Zhan, J., B. D. L. Fitt, H. O. Pinnschmidt, S. J. P. Oxley, and A. C. Newton. 2008. "Resistance, Epidemiology and Sustainable Management of *Rhynchosporium secalis* Populations on Barley." *Plant Pathology* 57: 1–14.

Zhang, X., N. Nguyen, S. Breen, et al. 2016. "Production of Small Cysteine-Rich Effector Proteins in *Escherichia coli* for Structural and Functional Studies." *Molecular Plant Pathology* 18: 141–151.

Zhang, X., B. Ovenden, and A. Milgate. 2020. "Recent Insights Into Barley and *Rhynchosporium commune* Interactions." *Molecular Plant Pathology* 21: 1111–1128.

Zhang, X., B. Ovenden, B. A. Orchard, et al. 2019. "Bivariate Analysis of Barley Scald Resistance With Relative Maturity Reveals a New Major QTL on Chromosome 3H." *Scientific Reports* 9: 20263.

Supporting Information

Additional supporting information can be found online in the Supporting Information section.